Polymer 204 (2020) 122815

Contents lists available at ScienceDirect

Polymer

journal homepage: http://www.elsevier.com/locate/polymer

Application of two Cu(II)-azido based 1D coordination polymers in optoelectronic device: Structural characterization and experimental studies

Monotosh Mondal [a,d], Sumanta Jana [b], Michael G.B. Drew [c], Ashutosh Ghosh [a,*]

[a] Department of Chemistry, University College of Science, University of Calcutta, 92, A.P.C. Road, Kolkata, 700 009, India
[b] Department of Chemistry, Jadavpur University, Jadavpur, Kolkata, 700 032, India
[c] School of Chemistry, The University of Reading, P.O. Box 224, Whiteknights, Reading, RG6 6AD, UK
[d] Department of Chemistry, Haldia Government College, Debhog, Purba Medinipur, 721657, India

ARTICLE INFO

Keywords:
1D polymeric chains
optical study
optoelectronic device
Schottky barrier diode

ABSTRACT

Two new azido bridged 1D polymeric Cu(II) chains, $[Cu(L^1)(\mu_{1,3}\text{-}N_3)]_\infty$ (**1**) and $[Cu_2(L^2)_2(\mu_{1,1}\text{-}N_3)(\mu_{1,3}\text{-}N_3)]_\infty$ (**2**) have been synthesized by using two different N_2O donor tridentate reduced Schiff base ligands, HL^1 = 2-[(2-dimethylamino-ethylamino)-methyl]-4-nitrophenol, HL^2 = 2-[(2-diethylamino-ethylamino)-methyl]-4-nitrophenol and both are structurally characterized. Cu(II) ions in both complexes occupy distorted pentacoordinated square pyramidal geometry. Both structures form polymeric chains, in **1**, *via* $\mu_{1,3}$-N_3^- while in **2** *via* both $\mu_{1,1}$-N_3^- and $\mu_{1,3}$-N_3^- bridges. The band gaps of the complexes (2.91 eV for **1** and 2.89 eV for **2**) suggest that both polymeric chains are semiconducting and thus possess the potential for uses in devices. A detail *I–V* analysis was performed to measure device related parameters i.e. effective carrier mobility, transit time, carrier concentration, diffusion length and ideality factor. The results show that both polymeric chains behave as Schottky barrier diodes (SBD) and could be used in opto-electronic device. Between the two complexes, **2** performs better than **1** in terms of applicability as indicated by the calculated parameters.

1. Introduction

During the past few decades, applications of coordination polymers (CPs) in the field of chemistry and material science are one of the fastest growing areas of research [1–6]. Coordination polymers are fascinating, highly ordered, flexible solid hybrid materials formed by metal ions/cluster of metal ions and organic ligands in an extended array [7,8]. Different structural dimensionality makes those compounds applicable in wide range of field *e.g.* device fabrication, magnetic materials, gases absorption and separation, ion exchange, drug delivery, catalysis, sensing of targeted molecules [9–20]. Another eye-catching feature of coordination polymers is their application in electronics and opto-electronic devices such as photovoltaic cells, Schottky barrier diodes (SBD) etc [21–25]. However, there are several limitations that arise from short transit time, high barrier potential, low thermal stability etc., that need to be checked before making any final device. Electrical conductivity, charge mobility, band gap and charge activation energy also play a vital role to make an efficient Schottky barrier diode. The properties of CPs depend on selection of metal ion and the flexibility and chemical functionality of the ligands. Choice of linkers and their steric and electronic nature play an important role to tune electronic properties [26,27]. Li et al. and Xia et al. had fabricated SBD devices using carboxylate linkers and d^{10} metal ions (Zn^{2+}, Cd^{2+}) those exhibit normal semiconductor properties [28,29]. To fabricate effective SBD devices, one has to be cautious about band gap engineering but fortunately the band gap of CPs can be tuned by controlling the size and conjugation of organic linker. Increasing size or extending π conjugation of organic linkers narrow down band gaps effectively [30]. It is really difficult to avoid all these limitations to prepare successful semiconducting CPs. Nevertheless, several highly ordered CPs have been synthesized, that assist band transport by high charge mobility [31–33].

On the other hand, N_2O donor Schiff base ligands have been widely used for synthesizing various homonuclear polymeric coordination complexes in the presence of different co-ligands like azido, thiocyanato, cyanato, carboxylato etc [34–36]. Among them Cu(II)-azido coordination complexes are one of the most interesting and popular systems for chemists due to their versatile structural dimensionality (discrete to three dimensional) and flexibility of Cu(II) ions in coordination numbers and geometries [37–39]. Although the magnetic properties of Cu(II)-azide polymeric chains have been well explored during the last

* Corresponding author.
E-mail address: agchem@caluniv.ac.in (A. Ghosh).

https://doi.org/10.1016/j.polymer.2020.122815
Received 23 March 2020; Received in revised form 18 June 2020; Accepted 13 July 2020
Available online 23 July 2020

decades, the application of these types of polymeric complexes in optoelectronics systems (Schottky barrier diodes (SBD), photovoltaic cells) and semiconductors have been relatively rare till now [40,41].

Herein, we report the synthesis of two new one dimensional polymeric chains of Cu(II) complexes, $[Cu(L^1)(\mu_{1,3}\text{-}N_3)]_\infty$ (**1**) and $[Cu_2(L^2)_2(\mu_{1,1}\text{-}N_3)(\mu_{1,3}\text{-}N_3)]_\infty$ (**2**) by using two different N_2O donor tridentate reduced Schiff base ligands (HL^1 = 2-[(2-dimethylamino-ethylamino)-methyl]-4-nitrophenol, HL^2 = 2-[(2-diethylamino-ethyl-amino)-methyl]-4-nitrophenol. The complexes are characterized by single crystal X-ray crystallography, electronic spectra, IR spectra and elemental analyses. We have thoroughly investigated the device parameters of **1** and **2** by fabricating SBD on ITO substrate. The measured device parameters suggest that **2** is more suitable as SBD than **1**.

2. Experimental section

2.1. Starting materials

2-hydroxy-5-nitrobenzaldehyde, N,N-dimethyl-1,2-ethylenediamine, N,N-diethyl-1,2-ethylenediamine and sodium borohydride were purchased from Spectrochem, India and were of reagent grade. They were used without further purification. The other reagents and solvents were of commercially available reagent quality, unless otherwise stated.

Caution! Although not encountered during experiment, perchlorate and azide salts of metal complexes with organic ligands are potentially explosive. Only a small amount of material should be prepared and should be handled with care.

2.2. Synthesis of the ligands 2-[(2-dimethylamino-ethylamino)-methyl]-4-nitrophenol (HL^1), 2-[(2-diethylamino-ethylamino)-methyl]-4-nitrophenol (HL^2)

The ligands, HL^1 and HL^2 were synthesized by refluxing 2-hydroxy-5-nitrobenzaldehyde (835.6 mg, 5 mmol) with N,N-dimethyl-1,2-ethylenediamine (0.55 mL, 5 mmol), N,N-diethyl-1,2-ethylenediamine (0.70 mL, 5 mmol)), respectively in methanol (30 mL) for 1 h. The methanolic solutions were cooled to 0 °C, and solid sodium borohydride (210 mg, 6 mmol) was added to both solutions slowly with constant stirring. After completion of the addition, the resulting reaction mixtures were acidified with concentrated HCl (5 mL) and then evaporated to dryness. The reduced Schiff-base ligands (HL^1, HL^2) were extracted from the solid residue with methanol. These methanolic solutions were used for preparation of complexes.

2.3. Syntheses of the complexes $[Cu(L^1)(\mu_{1,3}\text{-}N_3)]_\infty$ (**1**), $[Cu_2(L^2)_2(\mu_{1,1}\text{-}N_3)(\mu_{1,3}\text{-}N_3)]_\infty$ (**2**)

$Cu(ClO_4)_2{\cdot}6H_2O$ (370 mg, 1 mmol), dissolved in 15 mL methanol, was added to methanolic solution of previously prepared 1 mmol; HL^1 as described above with constant stirring. An aqueous solution (5 mL) of excess NaN_3 (130 mg, 2 mmol) was slowly added with continuous stirring. Now the whole solution was refluxed for 1 h. A deep blue solution was formed with little fine crystalline precipitate. After filtration, the solution was kept in open air. Reddish coloured needles of complex **1**, suitable for single crystal diffraction were obtained by slow evaporation of this filtrate. Complex **2** was synthesized following the same procedure, using HL^2.

Complex **1:** Yield: 0.22 g; (65%). Anal. Calcd. For $C_{11}H_{16}CuN_6O_3$ (343.85): C, 38.43; H, 4.69; N, 24.44. Found: C, 38.50; H, 4.74; N, 24.52. IR (KBr pellet, cm^{-1}): $\nu_{(N-H)}$, 3171 cm^{-1}, $\nu(N_3^-)$, 2078 and 2048 cm^{-1}.

Complex **2:** Yield: 0.52 g; (70%). Anal. Calcd. For $C_{26}H_{40}Cu_2N_{12}O_6$ (743.78): C, 41.99; H, 5.42; N, 22.60 Found: C, 42.18; H, 5.64; N, 22.73. IR (KBr pellet, cm^{-1}): $\nu_{(N-H)}$, 3276 cm^{-1}, $\nu(N_3^-)$, 2071 and 2053 cm^{-1}.

2.4. Physical measurements

Elemental analyses (C, H and N) were performed using a PerkinElmer 2400 series-II elemental analyzer. IR spectra in KBr pellets (4500–500 cm^{-1}) were recorded using a PerkinElmer RXI FT-IR spectrophotometer. Electronic spectra (1500–250 nm) were recorded in a Hitachi U-3501 spectro-photometer. The morphology of complexes is measured by field emission scanning electron microscope (FESEM).

2.5. X-ray crystallographic data collection and refinement

The crystallographic data of complexes **1**–**2** were collected as described earlier [42–44]. The crystals were mounted for data collection on a Bruker-AXS SMART APEX II diffractometer equipped with graphite monochromated Mo-Kα (λ = 0.71073 Å) radiation. The crystals were positioned at 60 mm from the CCD and 360 frames were measured with a counting time of 5 s. The structures were solved using direct methods with the SHELXT 2014/4 program [45]. The non-hydrogen atoms were refined with anisotropic thermal parameters. The hydrogen atoms bonded to carbon were included in geometric positions and given thermal parameters equivalent to 1.2 times (1.5 for methyl hydrogens) those of the atom to which they were attached. Absorption corrections were carried out by SADABS program [46]. In complex **2**, two atoms namely N(33) and C(34) were disordered over two positions which were refined with populations x and 1-x, with x refining to 0.44(2). The structure was twinned with BASF refining to 0.057(16). Both structures were refined on F^2 using Shelxl16/6 [47,48]. Details of the crystallographic data are summarized in Table 1. CCDC-1979815 (1), CCDC-1979816(2) contain the supplementary crystallographic data which can be obtained free of charge from The Cambridge Crystallographic Data Centre via www.ccdc.cam.ac.uk/data_request/cif.

2.6. Thin film fabrication from the precursor complexes

For optimum use and easy calculations of device parameters, thin films of the complexes are prepared. The thin film techniques have been used successfully to fabricate optoelectronic devices, electrodes, sensors etc. In this work, both complexes were deposited on ITO substrates (resistance ~ 10 Ω/sq cm, surface area 1.0 × 1.0 cm^2) by spin-coating method. ITO substrates were properly cleaned using following steps. They were washed first in soap-water and then with running distilled

Table 1
Crystallographic parameters for complexes **1** and **2**.

Complex	1	2
Chemical formula	$C_{11}H_{16}CuN_6O_3$	$C_{26}H_{40}Cu_2N_{12}O_6$
Formula weight	343.85	743.78
Crystal system	Monoclinic	Monoclinic
Space group	$P2_1/c$	$P2_1$
a(Å)	13.506(2)	7.858(5)
b (Å)	10.8408(19)	11.056(5)
c (Å)	9.7941(18)	18.042(5)
β, deg	102.119(2)	95.632(5)
V (Å3)	1402.0(4)	1559.9(13)
Z	4	2
ρ_{calc}(g cm^{-3})	1.629	1.584
μ (Mo Kα) (mm-1)	1.578	1.425
F(000)	708	772
Reflections collected	9513	11,548
Independent reflections	2503	5856
Reflections with I > 2σ(I)	1920	5295
R_1[a], wR_2[b]	0.0332, 0.0794	0.0360, 0.0895
GOF[c]	1.066	1.042
Residual electron Density, e/Å^{-3}	−0.350, 0.324	−0.355, 0.904

[a] $R_1 = \sum||F_o|-|F_c||/\sum|F_o|$.
[b] $wR_2\ (F_o^2) = [\sum[w(F_o^2 - F_c^2)^2/\sum w\ F_o^4]^{½}$ and.
[c] $GOF = [\sum[w(F_o^2 - F_c^2)^2/(N_{obs} - N_{params})]^{½}$

water. Now, these were sonicated for 1 h and degreased with 1:1 NH_3 and isopropanol vapour. Then the substrates were dried for 2 h in a hot air oven. About 3–4 mg of each composite were then dispersed in DMF in the ratio 1:4 and ultrasonicated for an hour. Now, a few drops of this solution were dropped onto the centre of clean ITO and spun at 600 rpm and then 1200 rpm for 3 and 5 min, respectively. The resulting films were dried in inert atmosphere and kept in desiccators.

3. Results and discussion

3.1. Syntheses of the complexes

The monocondensed tridentate reduced Schiff base ligands HL^1 and HL^2 have been synthesized by reported methods [49,50]. Both these ligands, on reaction with $Cu(ClO_4)_2{\cdot}6H_2O$ and NaN_3 in 1:1:2 M ratios produce two 1D polymeric chains $[Cu(L^1)(\mu_{1,3}\text{-}N_3)]_\infty$ (**1**), $[Cu_2(L^2)_2(\mu_{1,1}\text{-}N_3)(\mu_{1,3}\text{-}N_3)]_\infty$ (**2**) in CH_3OH-H_2O mixed solvent (10:1,v/v) (Scheme 1).

3.2. IR spectra of the complexes

Complexes **1** and **2** show moderately strong and sharp peaks at 3171 and 3276 cm^{-1}, respectively, ascribed to the symmetric stretching vibration of the amine (N–H) group. The absence of a typically strong and sharp peak due to the imine bond vibration in the range of 1620–1650 cm^{-1} confirms that the Schiff base ligand has been reduced. Both these data clearly indicate the reduction of the (>C═N–) moiety in the complexes [51–53]. In addition, the presence of (N_3^-) azido ligands in both complexes is confirmed by the appearance of strong and sharp peaks at 2078 cm^{-1} in **1** and 2071, 2053 cm^{-1} in **2**.

3.3. Description of the crystal structures

The X-ray crystal structure shows that complex **1** is a $\mu_{1,3}$-N_3^- bridged 1D polymeric chain based on asymmetric $[(CuL^1)(\mu_{1,3}\text{-}N_3)]$ unit (Fig. 1). In the chain, the copper atom [Cu(1)] occupies pentacoordinated square pyramidal geometry. Three donor atoms, secondary amine nitrogen atoms, N(18), N(21) and phenoxido oxygen atom, O(10) from the uninegative chelating tridentate ligand $(L^1)^-$ along with the N(1) atom of an azide ion constitute the basal plane with expected bond distances in the range of 1.943(2)-2.062(2) Å. Another N atom N(3)^b; $^b = x, 1/2\text{-}y, 1/2+z$] of the azide group from a neighbouring unit coordinates in the axial position at a distance of 2.405(3) Å to complete the square pyramidal geometry and to form the $\mu_{1,3}$-azido bridged 1D chain (Fig. 1). The basal Cu–N bond distances are longer than the basal Cu–O distances. The range of *cis* and *trans* angles around this Cu centre are in the range of [85.38(9)°–102.23(11)°], [170.03(11)°–170.12(9)°] respectively. The deviation of the geometry between square pyramidal and trigonal bipyramidal is calculated by the Addison parameter (τ). The value of τ is defined as the difference between the two largest donor-metal-donor angles divided by 60, τ is 0 for the ideal square pyramid and 1 for the trigonal bipyramid. The τ value of Cu(1) is 0.0, indicating that the geometry around Cu centre is square pyramid. The r.m.s. deviation of the four basal donor atoms of Cu(1) from their mean coordination plane is 0.011 Å with metal ion placed 0.161(1) Å away from the plane towards the N(3)^b atom. Hydrogen bonds are formed between N(18)–H(18) and O(10) in adjacent molecules in the 1D chain (Fig. S1). Selected bond distances, angles and hydrogen bond parameters are given in Tables S3 and S4 respectively.

Complex **2** also possesses a 1D polymeric chain structure but here the chain is formed by alternating $\mu_{1,3}$-N_3 and $\mu_{1,1}$-N_3 bridges in repeating fashion. The formula of the asymmetric unit is $[(CuL^2)(\mu_{1,3}\text{-}N_3)(CuL^2)N_3]$. Here also, both Cu(II) centres are penta-coordinated with distorted square pyramidal geometry (Fig. 2). The basal plane around Cu(1) is formed by two amine nitrogen atoms [N(18), N(21)], one phenoxido oxygen atom [O(10)] of tridentate reduced Schiff base ligand $(L^2)^-$ and one nitrogen atom [N(1)] of $\mu_{1,3}$-azido (N_3^-) ion with bond distances in the range of 1.935(3)–2.113(4) Å. The axial position is occupied by a nitrogen atom [N(4)^b] ($^b = 1+x,y,z$) of a $\mu_{1,1}$ bridged azido ion from a neighbouring unit with bond distance of 2.496(5) Å. The range of *cis* and *trans* angles around this Cu centre are in the range of [85.38(18)°–106.04(15)°], [156.39(18)°–175.33(19)°], respectively. The Addison

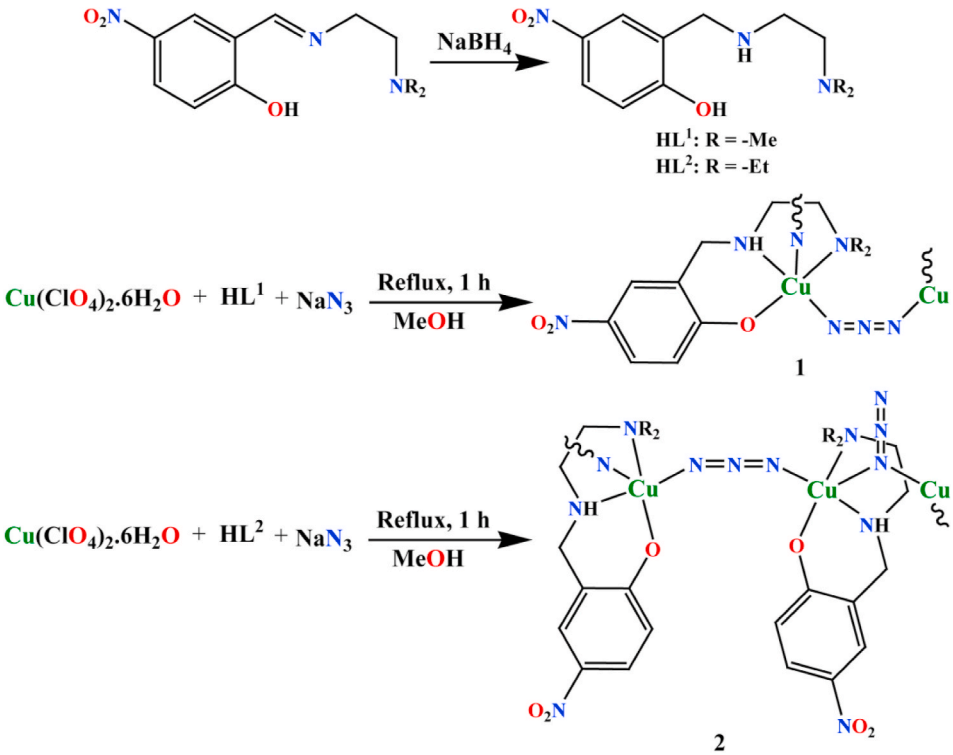

Scheme 1. Syntheses of complexes **1** and **2**.

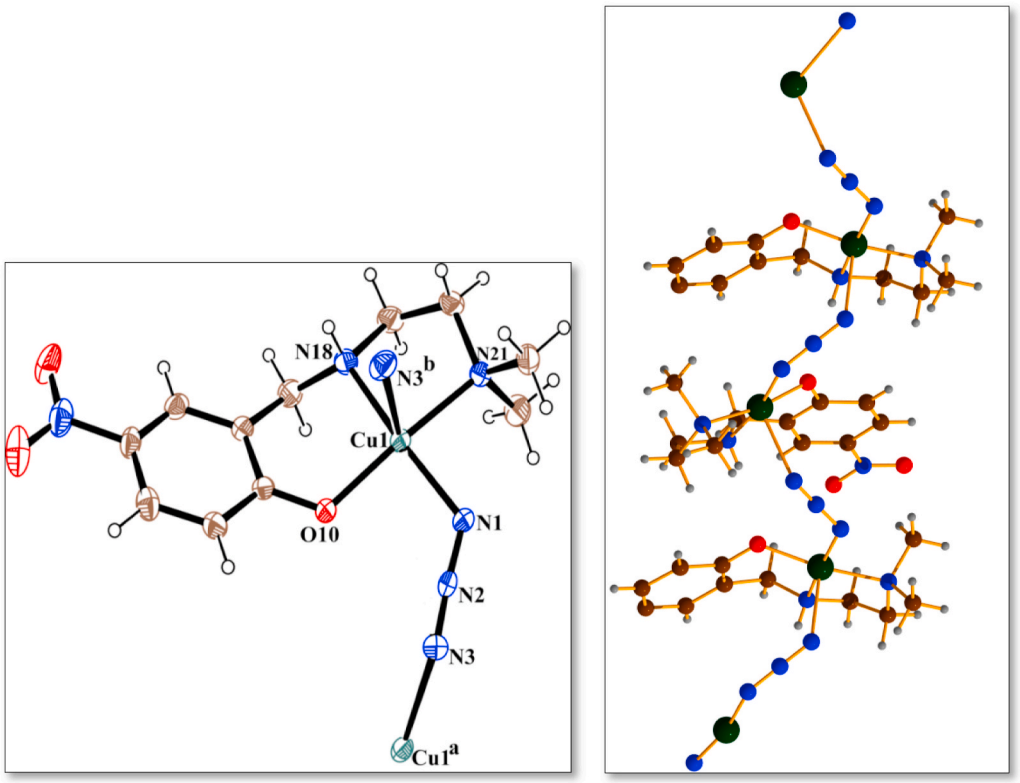

Fig. 1. The structure of **1** with ellipsoids at 30% probability. ([a] = *x, 1/2-y, -1/2+z*, [b] = *x, 1/2-y, 1/2+z*) (left); Chain structure of coordination polymer **1** (right).

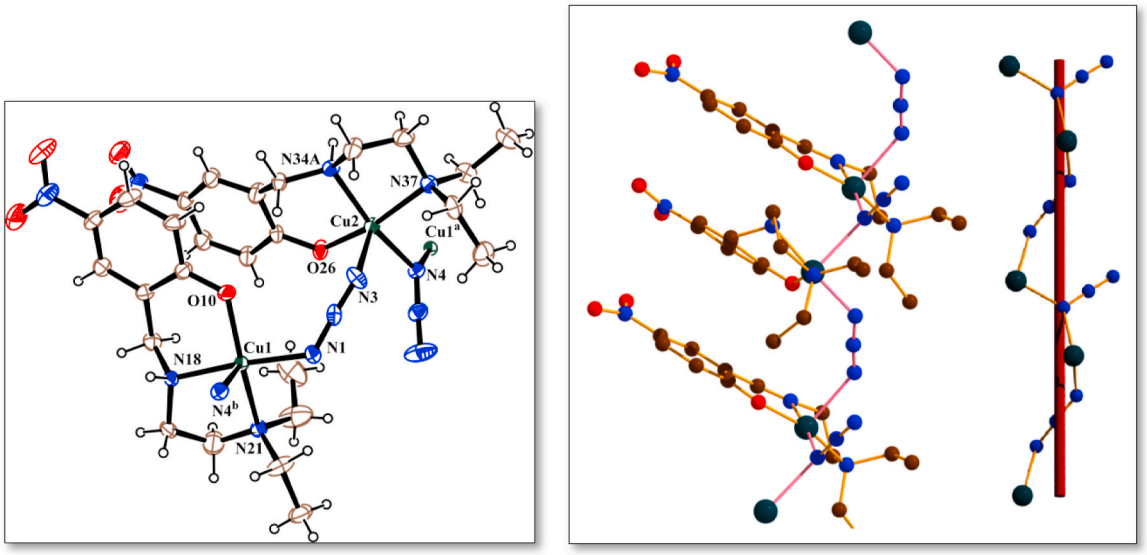

Fig. 2. The structure of **2** with ellipsoids at 30% probability. ([a] = *-1+x, y, z*, [b] = *1+x, y, z*) (left); M-type helical structure of complex **2** (right).

parameter (τ) of 0.316 for Cu(1) suggests that the geometry is significantly distorted from ideal square pyramidal towards trigonal pyramidal. The distortion around Cu(1) is also apparent from the r.m.s. deviation (0.221 Å) of the four equatorial donor atoms from their mean coordination plane and the metal ion is 0.188(2) Å away from the plane towards axial N(4)[b] atom.

The basal plane around Cu(2) is constituted by two amine nitrogen atoms [a disordered N(34) refined over two sites named N(34A) and N (34B) with occupancies 0.44(2), 0.56(2) respectively, and an ordered N (37)], one phenoxido oxygen atom [O(26)] of tridentate reduced Schiff base ligand $(L^2)^-$ and one nitrogen atom [N(4)] of $\mu_{1,1}$ bridged azido $(N_3)^-$ anion with bond distances in the range of 1.952(4)–2.114(4) Å. One nitrogen atom [N(3)] of $\mu_{1,3}$–azido ion occupies the axial position at 2.363(5) Å. The range of cis [85.38(18))–98.84(18)°] and trans angles [165.12(17)–176.0(3)°] around Cu(2) atom indicates the presence of distortion from the ideal square pyramidal geometry similar to that found around Cu(1). Because of the disorder in the position of N(34), two different values of the Addison parameter (τ) were calculated to be 0.033, 0.181 using N(34A) or N(34B) as part of the coordination respectively. Values concerning the equatorial plane were also different dependent on whether N(34A) or N(34B) were included with r.m.s. deviations of 0.022, 0.153 Å and the with the metal ion deviating by

0.272(4), 0.106(2) from the plane towards the N(3) atom. The chirality comes in **2** from helical structures *e.g.* P (right-handed helix) and M (left handed-helix) of polymeric chains. Complex **2** forms M-type of helix but it crystallizes as a conglomerate in chiral space group $P2_1$.There is a strong hydrogen bond between N(18)-H and O(26)[b] concurrent with the polymer formation. Because of the disorder, it is difficult to assess possible hydrogen bonds involving N(34) but there is no such bond in the polymer. However a weak such bond is observed for N(34A) with O (105) (*1-x*, *-1/2+y*, *1-z*) but not for N(34B) (Fig. S2). Selected bond distances, angles and hydrogen bond parameters are given in Tables S3 and S4, respectively.

3.4. Optical study

Fig. 3 (a) and (b) represent the UV–Visible absorption spectra of **1** and **2,** respectively. Very similar spectra are obtained for the complexes. Both complexes show sharp rise of the absorption peaks around 460 nm and also show maximum absorption at 372 nm. The band gap energy was calculated from the conventional Tauc's relation

$$(\alpha h\nu) \infty (h\nu\text{-}E_g)^n \quad (1)$$

where, photon energy; E_g, band gap energy; α, absorption coefficient; n, coefficient for direct band-to-band transition of value ½. Optical band gap was calculated by plotting $(\alpha h\nu)^2$ *vs.* hν and extrapolating the straight line to the x-axis. The band gap (E_g) was calculated as 2.91 and 2.89 eV for complexes **1** and **2,** respectively. These values suggest that changing of ligands has no impact in band structure because the complexes were synthesized by using similar N_2O donor reduced Schiff base ligands and azido (N_3^-) as bridging ligand. As both materials possess a wide band gap, this provides a good indication of useful device making properties.

3.5. Morphological analysis

Fig. 4 (a) shows a FESEM image of a thin film of complex **1** where randomly oriented flakes are grown with individual coarse islands. It shows porous morphology with several randomly oriented flakes, some of which have shallow cavities. Though the flakes are distinct, it is not possible to measure the size of grains due to agglomeration. On the other hand, complex **2** [Fig. 4 (b)] shows uniform granular morphology throughout the substrate and forms a nano bed. Average size was calculated to be 70–80 nm. Very few agglomerated particles are observed but overall morphology is uniform and compact. No pores have been found.

3.6. Electrical properties of devices

Two-probe *I–V* measurements were carried out by taking ITO coated glass substrates as the bottom contact and Al as the top contact (ITO/complex/Al). Experiments were carried out with Keithley 4200 in dark and under 1 Sun light illumination in the voltage range of −1 to +1 V. Fig. 5 shows *I–V* nature for complexes **1** and **2,** respectively. Evidently, the *I–V* characteristic curve of **2** exhibits enhanced nonlinear rectifying behavior compared to **1**. The nonlinearity of the I–V curve indicates the conduction mechanism is non-ohmic in nature for both coordination polymers and rectifying nature infers schottky barrier diode characteristics. Room temperature conductivity of **1** under dark and light conditions has been calculated as 12.54×10^{-5} S cm^{-1} and 20.94×10^{-5} S cm^{-1} respectively, whereas for **2** the values are 13.45×10^{-5} S cm^{-1} and 28.14×10^{-5} S cm^{-1} respectively. It is clearly shown that the conductivity has been increased for both polymeric substances under illumination condition. Now thermionic emission theory has been followed to get better realization of charge transportation [54]. The *I–V* plots are quantitatively analyzed and all parameters are verified using Cheung's equation

$$I = I_0 \left[exp\left(\frac{qV}{\eta kT}\right) - 1 \right] \quad (2)$$

where, I represents forward current, I_0; reverse saturation current, V; applied potential, q; electronic charge, K; Boltzmann constant, T; absolute temperature and η; ideality factor. The saturation current I_0 can be derived from the intercept of ln(I) at V = 0 and is given by

$$I_0 = AA^* T^2 \exp\left(\frac{-q\Phi_B}{KT}\right) \quad (3)$$

where, ϕ_B represents barrier height, A; effective diode area, and A* is effective Richardson constant, respectively. The effective diode area was maintained as 8.0×10^{-2} cm^2, and the effective Richardson constant was considered as 32 A K^{-2} cm^{-2} for all the devices. Now, forward *I–V* characteristics can be expressed as

$$I = I_0 \left[exp\left(\frac{q(V - IR_s)}{\eta kT}\right) \right] \quad (4)$$

where, the IR_S is the voltage drop across the series resistance that can be determined from the following equation

$$\frac{dV}{d(lnI)} = \frac{\eta kT}{q} + IR_s \quad (5)$$

Equation (5) also can be expressed as a function of 'I' as

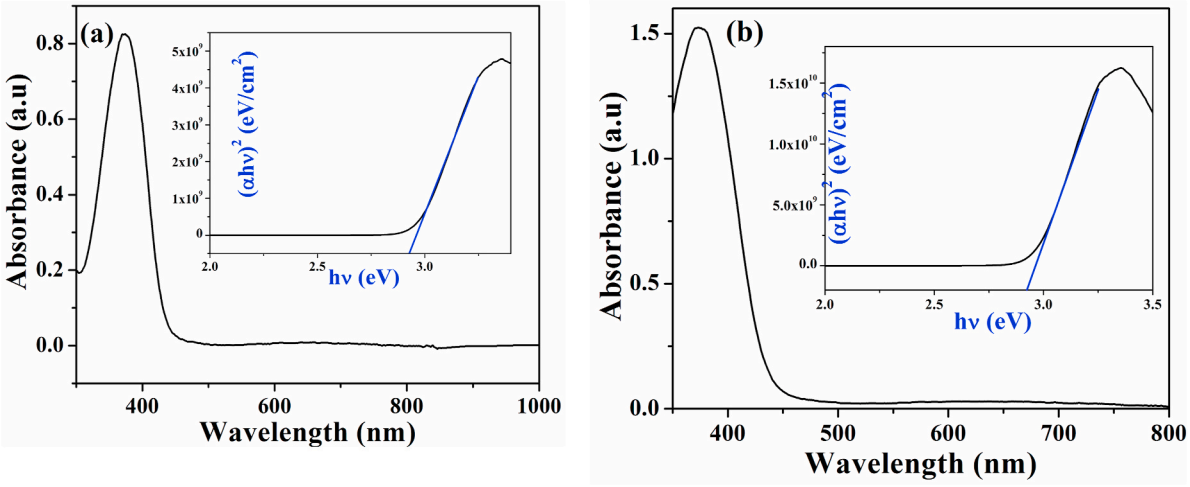

Fig. 3. UV–Vis spectrum of (a) complex **1,** inset: band gap of **1** (b) complex **2** and; inset: band gap of **2**.

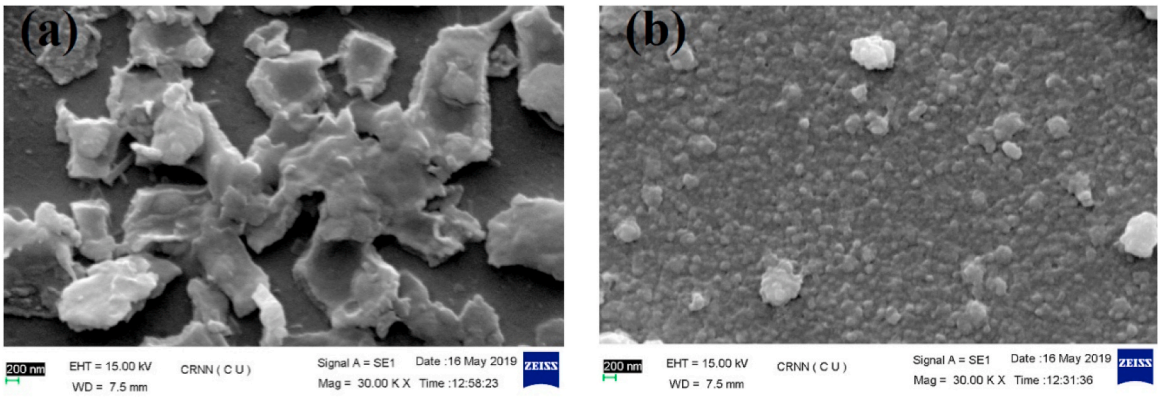

Fig. 4. FESEM images of (a) complex **1** and (b) complex **2**.

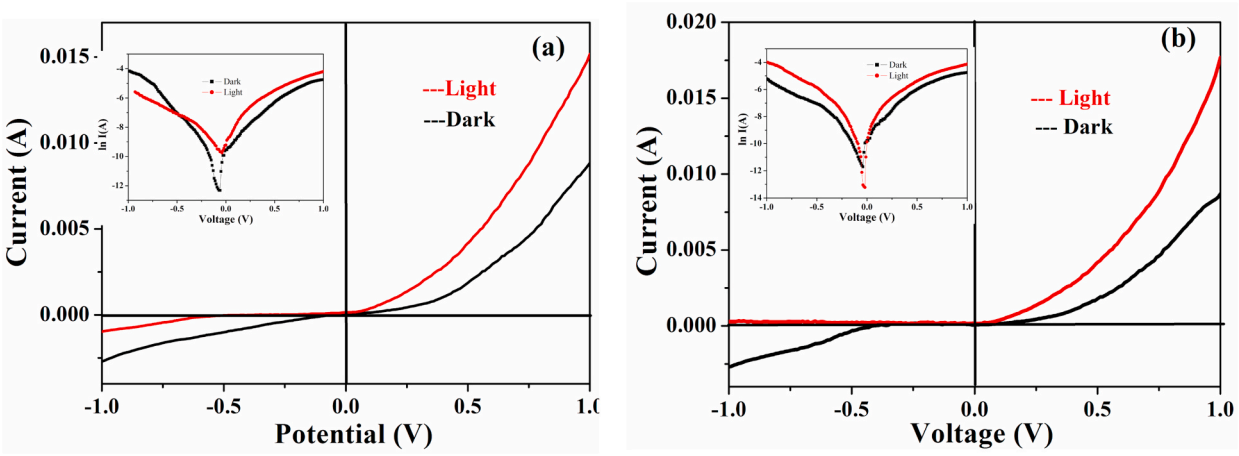

Fig. 5. *I–V* characteristic curve of (a) complex **1** under dark and illumination, inset: ln I *vs.* V plot; (b) complex **2** under dark and illumination, inset: ln I *vs.* V plot.

$$H(I) = IR_S + \eta\Phi_B \tag{6}$$

and H(I) can also be expressed as follows:

$$H(I) = V - \left(\frac{\eta kT}{q}\right)\ln\left(\frac{I}{AA^*T^2}\right) \tag{7}$$

The ideality factor (η) and series resistance (R_S) of two devices are calculated under dark and illumination conditions from the intercept and slope of dV/d(ln I) *vs.* I plots (Fig. 6). The resultant ideality factor (η) values are 2.25, 3.21 under dark condition and 1.59, 1.27 under illumination for coordination polymers **1** and **2,** respectively. The calculated η values suggest that the MS junctions of both complexes are not exactly ideal. This deviation originates from various reasons *e.g.* mismatch of interfacial states, in-homogeneities in Schottky barrier height and series resistance in the junction [55]. But complex **2** shows more ideality in device fabrication over **1**.

The potential barrier height (Φ_B) values are calculated from the intercepts of H(I) *vs.* I plots of both complexes **1** and **2** (Fig. 7). The values of 'H' are calculated by using η values (obtained from Fig. 6) in equation

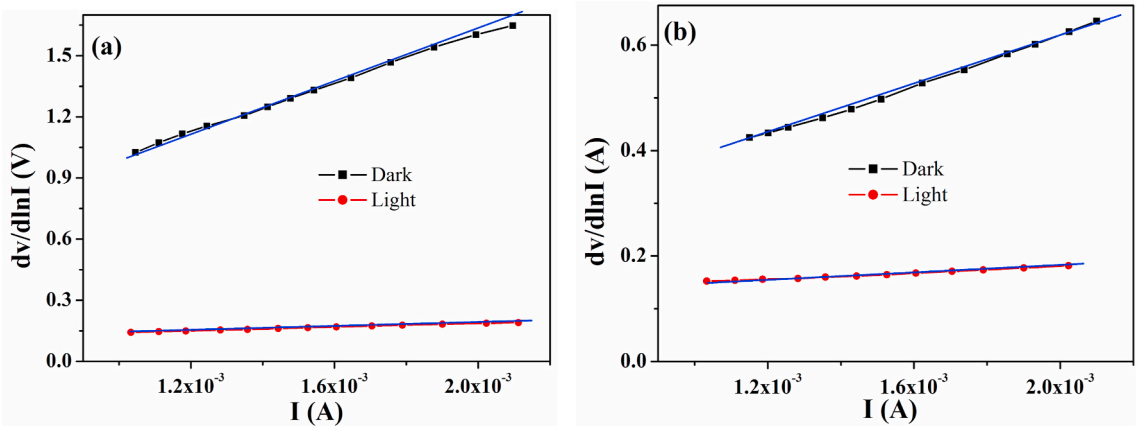

Fig. 6. dV/d(ln I) *vs.* I plot under dark and illumination conditions for (a) complex **1** and (b) complex **2**.

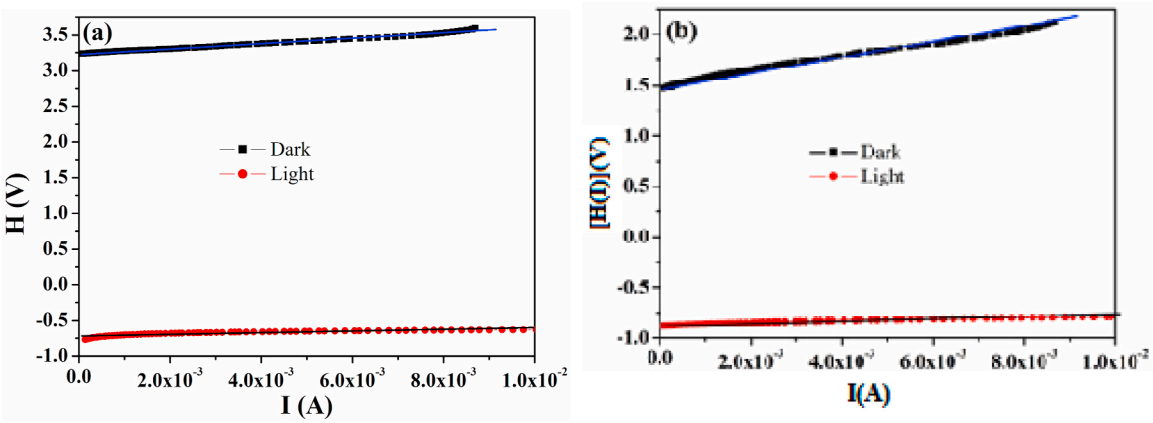

Fig. 7. H (I) *vs.* I graph under dark and illumination condition for (a) **1** and (b) **2** thin film devices, respectively.

(6). The plots of H (I) *vs.* I provide straight lines with the y-axis intercepts, which are equal to $\eta\Phi_B$ values. All the device related parameters *e.g.,* potential height (φ_B), ideality factor (η), and series resistance (R_S) are listed in Table S1 (for **1**) and Table S2 (for **2**).

Now SCLC theory has been introduced for detailed analysis of MS junctions in the light of charge transport phenomena. The application of SCLC theorem helps to calculate several important transport parameters *e.g.* effective carrier mobility (μ_{eff}), diffusion length (L_D), transient time (τ), carrier concentration etc. Fig. 8(a–d) represent log-log plot of complexes **1** and **2** under dark and illumination conditions. Both plots show two separate linear regions of different slopes, which suggest that two different conduction mechanisms are operating in MS junction. At low potential (region-I), the device exhibits an ohmic nature where, current is directly proportional to applied voltage ($I \propto V$). Region-I is attributed to thermionic emission where bulk generated electrons govern to produce current than the injected free carriers [56–58]. At higher bias, the *I–V* curve follows power law nature ($I \propto V^m$), where slope values (m) are determining factor to separate ohmic and SCLC regions. In case of the ohmic region, the slope is ≤ 1 whereas ≥ 2 for SCLC region [59]. Just after the region-I current becomes directly proportional to the square of applied voltage ($I \propto V^2$). Therefore in region-II, current is governed by space charge limited current (SCLC) and is also proportional to the square of applied bias [60,61]. Therefore, standard SCLC theory was applied here to get further insight into the charge

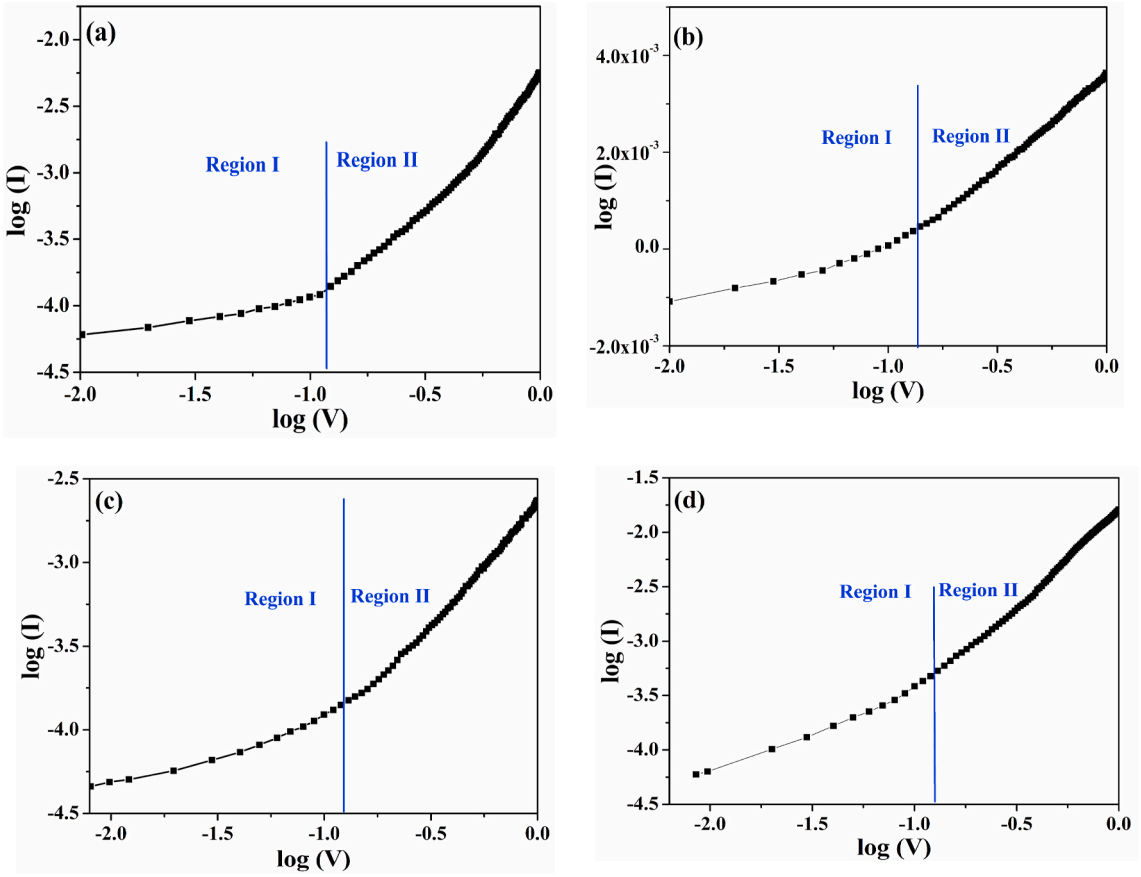

Fig. 8. log (I) *vs.* log (V) plot for complex **1** under (a) dark and (b) illumination conditions and log-log plot of complex **2** under (c) dark and (d) illumination conditions.

transfer process.

From the I *vs.* V^2 graph (Fig. S3) carrier mobility values have been evaluated by using the Mott−Gurney equation [62]:

$$J = \frac{9\mu_{eff}\varepsilon_0\varepsilon_r}{8}\frac{V^2}{d^3} \quad (8)$$

where J, ε_0, ε_r, μ_{eff} and d are current density, permittivity in free space, relative dielectric constant of CPs, effective carrier mobility and thickness of the film respectively. Before calculating μ_{eff}, dielectric constants for both complexes have been measured from the plots of capacitance *vs.* frequency (Fig. S4) with the help of following equation [63]:

$$\varepsilon_r = \frac{1}{\varepsilon_0}\cdot\frac{C.L}{A} \quad (9)$$

Here, C; saturation capacitance, L; film thickness, A; diode area, respectively. The calculated relative dielectric constants for complex **1** and **2** are 4.23 and 1.27, respectively. Relatively lower dielectric constant value of complex **2** ensures its potential use in opto-electronic device to minimize power loss.

Here thickness of the films is about 1 μm for both devices made by complexes **1** and **2**. Transit time (τ) of the charge carriers is another key parameter in analyzing charge transport across the junction. The τ values have been calculated from equation (10) with help of the slopes of forward *I–V* curves (Fig. 5) [64].

$$\tau = \frac{9\varepsilon_0\varepsilon_r A}{8d}\left(\frac{V}{I}\right) \quad (10)$$

Effective carrier mobilities and transit times for **1** and **2** are presented in Tables S1 and S2. Higher mobility value of **2** indicates easier electron transport through the MS junction compared to **1**. After light illumination, mobility enhancement of the carrier signifies a good photo-responsivity for this kind of polymeric semiconductor. These entire device related parameters imply the eventual superiority of complex **2** compared to complex **1**.

4. Conclusions

Two similar N_2O donor tridentate ligands on reaction with Cu $(ClO_4)_2{\cdot}6H_2O$, produce two new Cu(II) based 1D polymeric chains in presence of azido co-anion. Although the ligands are very similar, the connectivity in the chains are different: in **1** the Cu(II) centres are connected only by $\mu_{1,3}$-N_3 bridge whereas in **2** alternating $\mu_{1,1}$-N_3 and $\mu_{1,3}$-N_3 bridges are present. The semiconducting nature of both the chains is evident from their wide electronic band gaps. The *I–V* characteristics of complexes **1** and **2** show non-linear rectifying properties under illumination condition, suggesting Schottky Barrier Diodes characteristics. Measurements of different device parameters like carrier mobility, transit time, and diffusion length, barrier height, ideality factor show that both polymeric complexes are promising material for SBD devices and device applicability of **2** is better than that of **1**.

Declaration of competing interest

The authors declare that they have no known competing financial interests or personal relationships that could have appeared to influence the work reported in this paper.

CRediT authorship contribution statement

Monotosh Mondal: Investigation, Methodology, Writing - original draft. **Sumanta Jana:** Formal analysis, Visualization. **Michael G.B. Drew:** Writing - review & editing. **Ashutosh Ghosh:** Conceptualization, Supervision, Writing - review & editing.

Declaration of competing interest

The authors declare that they have no known competing financial interests or personal relationships that could have appeared to influence the work reported in this paper.

Acknowledgment

A. G. thanks the DST-FIST funded single crystal X-ray diffractometer facility at the department of chemistry, University of Calcutta for providing the single crystal X-ray diffractometer facility. Sumanta Jana acknowledges UGC India for offering him Dr. D. S. Kothari Postdoctoral Fellowship [Award letter no. F.4-2/2006 (BSR) /CH/18–19/0017].

Appendix A. Supplementary data

Supplementary data to this article can be found online at https://doi.org/10.1016/j.polymer.2020.122815.

References

[1] M.H. Mir, L.L. Koh, G.K. Tan, J.J. Vittal, Single-crystal to single-crystal photochemical structural transformations of interpenetrated 3D coordination polymers by [2+2] cycloaddition reactions, Angew. Chem. Int. Ed. 49 (2010) 390–393, https://doi.org/10.1002/anie.200905898.

[2] L.K. Das, C.J. Gómez-García, A. Ghosh, Influence of the central metal ion in controlling the self-assembly and magnetic properties of 2D coordination polymers derived from $[(NiL)_2M]^{2+}$ nodes (M= Ni, Zn and Cd) (H^2L= salen-type di-Schiff base) and dicyanamide spacers, Dalton Trans. 44 (2015) 1292–1302, https://doi.org/10.1039/c4dt02823f.

[3] L.K. Das, C. Diaz, A. Ghosh, Antiferromagnetic mixed-valence Cu(I)–Cu(II) two-dimensional coordination polymers constructed by double oximato bridged Cu(II) dimers and Cu^ISCN based one-dimensional anionic chains, Cryst. Growth Des. 15 (2015) 3939–3949, https://doi.org/10.1021/acs.cgd.5b00560.

[4] T. Yamada, K. Otsubo, R. Makiura, H. Kitagawa, Designer coordination polymers: dimensional crossover architectures and proton conduction, Chem. Soc. Rev. 42 (2013) 6655–7044, https://doi.org/10.1039/C3CS60028A.

[5] H. Li, Y. Wang, Y. He, Z. Xu, X. Zhao, Y. Han, Synthesis of several novel coordination complexes: ion exchange, magnetic and photocatalytic studies, New J. Chem. 41 (2017) 1046–1056, https://doi.org/10.1039/C6NJ02863B.

[6] P. Mahapatra, M.G.B. Drew, A. Ghosh, Variations of structures and phenoxazinone synthase-like activity of the complexes based on $(Cu^{II})_2Mn^{II}$ node and dicyanamide spacer, Cryst. Growth Des. 17 (2017) 6809–6820, https://doi.org/10.1021/acs.cgd.7b01407.

[7] C. Janiak, J.K. Vieth, MOFs, MILs and more: concepts, properties and applications for porous coordination networks (PCNs), New J. Chem. 34 (2010) 2366–2388, https://doi.org/10.1039/C0NJ00275E.

[8] N.N. Adarsh, P. Dastidar, Coordination polymers: what has been achieved in going from innocent 4,4′-bipyridine to bis-pyridyl ligands having a non-innocent backbone? Chem. Soc. Rev. 41 (2012) 3039–3060, https://doi.org/10.1039/C2CS15251G.

[9] D. Farrusseng, Metal–Organic Frameworks. Applications from Catalysis to Gas Storage, Wiley-VCH Verlag GmbH, Weinheim, 2011.

[10] K. Biradha, C.Y. Su, J.J. Vittal, Recent developments in crystal engineering, Cryst. Growth Des. 11 (2011) 875–886, https://doi.org/10.1021/cg101241x.

[11] S. Ganguly, P. Kar, M. Chakraborty, A. Ghosh, The first alternating Mn^{II}–Mn^{III} 1D chain: structure, magnetic properties and catalytic oxidase activities, New J. Chem. 42 (2018) 9517–9529, https://doi.org/10.1039/c8nj00414e.

[12] Z. Zhang, Y. Zhao, Q. Gong, Z. Li, J. Li, MOFs for CO_2 capture and separation from flue gas mixtures: the effect of multifunctional sites on their adsorption capacity and selectivity, Chem. Commun. 49 (2013) 653–661, https://doi.org/10.1039/C2CC35561B.

[13] T. Kundu, S. Mitra, P. Patra, A. Goswami, D. Díaz Díaz, R. Banerjee, Mechanical downsizing of a gadolinium (III)-based metal–organic framework for anticancer drug delivery, Chem. Eur. J. 20 (2014) 10514–10518, https://doi.org/10.1002/chem.201402244.

[14] P. Kar, P.M. Guha, M.G.B. Drew, T. Ishida, A. Ghosh, Spin-canted antiferromagnetic phase transitions in alternating phenoxo- and carboxylato-bridged Mn^{III}-Salen complexes, Eur. J. Inorg. Chem. 13 (2011) 2075–2085, https://doi.org/10.1002/ejic.201001215.

[15] S. Khan, S. Halder, P.P. Ray, S. Herrero, R. González-Prieto, M.G.B. Drew, S. Chattopadhyay, A semiconducting copper(II) coordination polymer with (4,4) square grid topology: synthesis, characterization, and application in the formation of a photoswitch, Cryst. Growth Des. 18 (2018) 651–659, https://doi.org/10.1021/acs.cgd.7b00830.

[16] S. Roy, A. Dey, P.P. Ray, J. Ortega-Castro, A. Frontera, S. Chattopadhyay, Application of a novel 2D cadmium (II)-MOF in the formation of a photo-switch with a substantial on–off ratio, Chem. Commun. 51 (2015) 12974–12976, https://doi.org/10.1039/c5cc04323a.

[17] Y. Zhang, J. Yang, D. Zhao, Z. Liu, D. Li, L. Fan, T. Hu, Two cadmium (II) coordination polymers as luminescent sensors for the detection of nitrofuran/nitroimidazole antibiotics, CrystEngComm 21 (2019) 6130–6135, https://doi.org/10.1039/C9CE01164A.

[18] L. Fan, Y. Zhang, J. Liang, X. Wang, H. Lv, J. Wang, L. Zhao, X. Zhang, Structural diversity, magnetic properties, and luminescence sensing of five 3D coordination polymers derived from designed 3, 5-di (2′, 4′-dicarboxylphenyl) benozoic acid, CrystEngComm 20 (2018) 4752–4762, https://doi.org/10.1039/C8CE00877A.

[19] J. Wang, N.N. Chen, C. Zhang, L.Y. Jia, L. Fan, Functional group induced structural diversities and photocatalytic, magnetic and luminescence sensing properties of four cobalt (II) coordination polymers based on 1, 3, 5-tris (2-methylimidazol-1-yl) benzene, CrystEngComm 22 (2020) 811–820, https://doi.org/10.1039/C9CE01474H.

[20] L. Fan, Z. Liu, Y. Zhang, F. Wang, D. Zhao, J. Yang, X. Zhang, Luminescence sensing, electrochemical, and magnetic properties of 2D coordination polymers based on the mixed ligands p-terphenyl-2, 2′′, 5′′, 5′′′-tetracarboxylate acid and 1, 10-phenanthroline, New J. Chem. 43 (2019) 13349–13356, https://doi.org/10.1039/C9NJ03530C.

[21] V. Stavila, A.A. Talin, M.D. Allendorf, MOF-based electronic and opto-electronic devices, Chem. Soc. Rev. 43 (2014) 5994–6010, https://doi.org/10.1039/C4CS00096J.

[22] A. Dhakshinamoorthy, H. Garcia, Catalysis by metal nanoparticles embedded on metal–organic frameworks, Chem. Soc. Rev. 41 (2012) 5262–5284, https://doi.org/10.1039/C2CS35047E.

[23] M.D. Allendorf, C.A. Bauer, R.K. Bhaktaa, R.J.T. Houka, Luminescent metal–organic frameworks, Chem. Soc. Rev. 38 (2009) 1330–1352, https://doi.org/10.1039/B802352M.

[24] S. Roy, S. Halder, M.G.B. Drew, P.P. Ray, S. Chattopadhyay, Fabrication of an active electronic device using a hetero-bimetallic coordination polymer, ACS Omega 3 (2018) 12788–12796, https://doi.org/10.1021/acsomega.8b02025.

[25] B. Dutta, R. Jana, A.K. Bhanja, P.P. Ray, C. Sinha, M.H. Mir, Supramolecular aggregate of Cadmium (II)-based one-dimensional coordination polymer for device fabrication and sensor application, Inorg. Chem. 58 (2019) 2686–2694, https://doi.org/10.1021/acs.inorgchem.8b03294.

[26] Y. He, B. Li, M. O'Keeffe, B. Chen, Multifunctional metal–organic frameworks constructed from meta-benzenedicarboxylate units, Chem. Soc. Rev. 43 (2014) 5618–5656, https://doi.org/10.1039/C4CS00041B.

[27] M.M. Lee, H.Y. Kim, I.H. Hwang, J.M. Bae, C. Kim, C.H. Yo, Y. Kim, S.J. Kim, Cd^{II} MOFs constructed using succinate and bipyridyl ligands: photoluminescence and heterogeneous catalytic activity, Bull. Korean Chem. Soc. 35 (2014) 1777–1783.

[28] W.J. Li, J. Liu, Z.H. Sun, T.F. Liu, J. Lü, S.Y. Gao, C. He, R. Cao, J.H. Luo, Integration of metal-organic frameworks into an electrochemical dielectric thin film for electronic applications, Nat. Commun. 7 (2016) 11830–11837, https://doi.org/10.1038/ncomms11830.

[29] T.K. Maji, R. Matsuda, S. Kitagawa, Integration of metal-organic frameworks into an electrochemical dielectric thin film for electronic applications, Nat. Mater. 6 (2007) 142–148, https://doi.org/10.1038/ncomms11830.

[30] C.H. Lee, J.Y. Wu, G.H. Lee, S.M. Peng, J.C. Jiang, K.L. Lu, Correlation of mesh size of metal–carboxylate layer with degree of interpenetration in pillared-layer frameworks, Cryst. Growth Des. 14 (2014) 5608–5616, https://doi.org/10.1021/cg500871d.

[31] K. Sinzger, S. Hünig, M. Jopp, D. Bauer, W. Bietsch, J.U. von Schütz, H.C. Wolf, R. K. Kremer, T. Metzenthin, R. Bau, S.I. Khan, A. Lindbaum, C.L. Lengauer, E. Tillmanns, The organic metal (Me2-DCNQI)2Cu: dramatic changes in solid-state properties and crystal structure due to secondary deuterium effects, J. Am. Chem. Soc. 115 (1993) 7696–7705, https://doi.org/10.1021/ja00070a013.

[32] R. Kato, H. Kobayashi, A. Kobayashi, T. Mori, H. Inokuchi, Preparation and structure of highly conductive anion radical salts, M (2,5-R_1, R_2-DCNQI$_2$)(DCNQI= N, N′-dicyanoquinonediimine; R_1, R_2= Me, MeO, halogen; M= Ag, Li, Na, K, NH_4), Synth. Met. 27 (1988) 263–268, https://doi.org/10.1016/0379-6779(88)90154-3.

[33] R. Kato, H. Kobayashi, A. Kobayashi, Crystal and electronic structures of conductive anion-radical salts, (2,5-R_1R_2-DCNQI)$_2$Cu (DCNQI= N, N′-dicyanoquinonediimine; R_1, R_2= CH_3, CH_3O, Cl, Br), J. Am. Chem. Soc. 111 (1989) 5224–5232, https://doi.org/10.1021/ja00196a032.

[34] M. Mondal, P.M. Guha, S. Giri, A. Ghosh, Deactivation of catecholase-like activity of a dinuclear Ni (II) complex by incorporation of an additional Ni (II), J. Mol. Catal. A Chem. 424 (2016) 54–64, https://doi.org/10.1016/j.molcata.2016.08.012.

[35] M. Mondal, S. Giri, P.M. Guha, A. Ghosh, Dependence of magnetic coupling on ligands at the axial positions of Ni^{II} in phenoxido bridged dimers: experimental observations and DFT studies, Dalton Trans. 46 (2017) 697–708, https://doi.org/10.1039/c6dt03855g.

[36] R. Biswas, C. Diaz, A. Bauzá, M. Barceló-Oliver, A. Frontera, A. Ghosh, Triple-bridged ferromagnetic nickel (II) complexes: a combined experimental and theoretical DFT study on stabilization and magnetic coupling, Dalton Trans. 43 (2014) 6455–6467, https://doi.org/10.1039/c3dt52764f.

[37] G. Lazari, T.C. Stamatatos, C.P. Raptopoulou, V. Psycharis, M. Pissas, S.P. Perlepes, A.K. Boudalis, A metamagnetic 2D copper (II)-azide complex with 1D ferromagnetism and a hysteretic spin-flop transition, Dalton Trans. (2009) 3215–3221, https://doi.org/10.1039/B823423J.

[38] Y.S. You, J.H. Yoon, H.C. Kimb, C.S. Hong, Chiral azide-bridged two-dimensional Cu(II) compounds showing a field-induced spin–flop transition, Chem. Commun. (2005) 4116–4118, https://doi.org/10.1039/B507051A.

[39] E.Q. Gao, S.Q. Bai, C.F. Wang, Y.F. Yue, C.H. Yan, Structural and magnetic properties of three one-dimensional azido-bridged copper(II) and manganese(II) coordination polymers, Inorg. Chem. 42 (2003) 8456–8464, https://doi.org/10.1021/ic034618w.

[40] S. Naiya, C. Biswas, M.G.B. Drew, C.J. Gomez-Garcia, J.M. Clemente-Juan, A. Ghosh, A unique example of structural and magnetic diversity in four interconvertible copper (II)−azide complexes with the same schiff base ligand: a monomer, a dimer, a chain, and a layer, Inorg. Chem. 49 (2010) 6616–6627, https://doi.org/10.1021/ic1005456.

[41] A. Hazari, C. Diaz, A. Ghosh, H-bond assisted coordination bond formation in the 1D chains based on azido and phenoxido bridged tetranuclear Cu (II) complexes with reduced Schiff base ligands, Polyhedron 142 (2018) 16–24, https://doi.org/10.1016/j.poly.2017.12.022.

[42] S. Maity, S. Ghosh, A. Ghosh, Elucidating the secondary effect in the Lewis acid mediated anodic shift of electrochemical oxidation of a Cu(II) complex with a N_2O_2 donor unsymmetrical ligand, Dalton Trans. 48 (2019) 14898–14913, https://doi.org/10.1039/C9DT03323H.

[43] T.K. Ghosh, P. Mahapatra, S. Jana, A. Ghosh, Variation of nuclearity in Ni^{II} complexes of a Schiff base ligand: crystal structures and magnetic studies, CrystEngComm 21 (2019) 4620–4631, https://doi.org/10.1039/C9CE00574A.

[44] S. Maity, P. Bhunia, K. Ichihashi, T. Ishida, A. Ghosh, SMM behaviour of heterometallic dinuclear Cu^{II} Ln^{III} (Ln= Tb and Dy) complexes derived from N_2O_3 donor unsymmetrical ligands, New J. Chem. 44 (2020) 6197–6205, https://doi.org/10.1039/D0NJ00193G.

[45] G.M. Sheldrick, ShelXL 2013, 2013.

[46] SAINT, Version 6.02, SADABS, Version 2.03, Bruker AXS Inc., Madison, WI, 2002.

[47] G.M. Sheldrick, Shelxs 97, Acta Crystallogr. Sect. A Found. Crystallogr. 64 (2008) 112, https://doi.org/10.1107/S0108767307043930.

[48] G.M. Sheldrick, Shelxl 2014, crystal structure refinement with SHELXL, Acta Crystallogr. Sect. C Struct. Chem. 71 (2015) 3–8, https://doi.org/10.1107/S2053229614024218.

[49] A. Biswas, L.K. Das, M.G.B. Drew, C. Diaz, A. Ghosh, Insertion of a hydroxido bridge into a diphenoxido dinuclear copper (ii) complex: drastic change of the magnetic property from strong antiferromagnetic to ferromagnetic and enhancement in the catecholase activity, Inorg. Chem. 51 (2012) 10111–10121, https://doi.org/10.1021/ic300319s.

[50] M. Mondal, J. Mayans, A. Ghosh, Formation of a carbonato bridged Ni_4-complex by atmospheric CO_2 fixation: crystal structure and magnetic properties, Inorg. Chim. Acta 498 (2019) 119175, https://doi.org/10.1016/j.ica.2019.119175.

[51] M. Mondal, M. Chakraborty, M.G.B. Drew, A. Ghosh, Ni(II) dimers of NNO donor tridentate reduced schiff base ligands as alkali metal ion capturing agents: syntheses, crystal structures and magnetic properties, Magnetochemistry 4 (2018) 51, https://doi.org/10.3390/magnetochemistry4040051.

[52] A. Biswas, M.G.B. Drew, C.J. Gomez-García, A. Ghosh, Use of a reduced schiff-base ligand to prepare novel chloro-bridged chains of rare Cu(II) trinuclear complexes with mixed azido/oxo and chloro/oxo bridges, Inorg. Chem. 49 (2010) 8155–8163, https://doi.org/10.1021/ic101183n.

[53] M. Mondal, S. Ghosh, S. Maity, S. Giri, A. Ghosh, In situ transformation of a tridentate to a tetradentate unsymmetric Schiff base ligand via deaminative coupling in Ni(II) complexes: crystal structures, magnetic properties and catecholase activity study, Inorg. Chem. Front 7 (2020) 247, https://doi.org/10.1039/c9qi00975b.

[54] E.H. Rhoderick, Metal Semiconductors Contacts, Oxford University Press, Oxford, U.K., 1978.

[55] R.K. Gupta, F. Yakuphanoglu, Photoconductive Schottky diode based on Al/p- Si/SnS_2/Ag for optical sensor applications, Sol. Energy 86 (2012) 1539–1545, https://doi.org/10.1016/j.solener.2012.02.015.

[56] Y.S. Ocak, M. Kulakci, T. Kılıcoğlu, R. Turan, K. Akkılıc, Current–voltage and capacitance–voltage characteristics of a Sn/Methylene Blue/p-Si Schottky diode, Synth. Met. 159 (2009) 1603–1607, https://doi.org/10.1016/j.synthmet.2009.04.024.

[57] R. Sahingoz, H. Kanbur, M. Voigt, C. Soykan, The determination of interface states and series resistance profile of Al/polymer/PEDOT-PSS/ITO heterojunction diode by IV and CV methods, Synth. Met. 158 (2008) 727–731, https://doi.org/10.1016/j.synthmet.2008.04.023.

[58] S. Aydoğan, M. Sağlam, A. Türüt, The temperature dependence of current–voltage characteristics of the Au/Polypyrrole/p-Si/Al heterojunctions, J. Phys. Condens. Matter 18 (2006) 2665–2676.

[59] A.A.M. Farag, W.A. Farooq, F. Yakuphanoglu, Characterization and performance of Schottky diode based on wide band gap semiconductor ZnO using a low-cost and simplified sol–gel spin coating technique, Microelectron. Eng. 88 (2011) 2894–2899, https://doi.org/10.1016/j.mee.2011.03.016.

[60] Z. Ahmad, M.H. Sayyad, Extraction of electronic parameters of Schottky diode based on an organic semiconductor methyl-red, Phys. E 41 (2009) 631–634, https://doi.org/10.1016/j.physe.2008.08.068.

[61] A. Jain, P. Kumar, S.C. Jain, V. Kumar, R. Kaur, R.M. Mehra, Trap filled limit voltage (V_{TFL}) and V^2 law in space charge limited currents, J. Appl. Phys. 102 (2007), https://doi.org/10.1063/1.2802553, 094505.

[62] P.W.M. Blom, M.J.M. de Jong, M.G. van Munster, Phys. Rev. B Condens. Matter Mater. Phys. 55 (1997) R656–R659.

[63] S. Suresh, Synthesis, structural and dielectric properties of zinc sulfide nanoparticles, Int. J. Phys. Sci. 8 (2013) 1121–1127, https://doi.org/10.5897/IJPS2013.3926.

[64] A. Dey, A. Layek, A. Roychowdhury, M. Das, J. Datta, S. Middya, D. Das, P.P. Ray, Investigation of charge transport properties in less defective nanostructured ZnO based Schottky diode, RSC Adv. 5 (2015) 36560–36567, https://doi.org/10.1039/C4RA16828C.